

Heterogeneous Graph Transformer for Multiple Tiny Object Tracking in RGB-T Videos

Qingyu Xu, Longguang Wang, Weidong Sheng, Yingqian Wang, Chao Xiao, Chao Ma, Wei An

Abstract—Tracking multiple tiny objects is highly challenging due to their weak appearance and limited features. Existing multi-object tracking algorithms generally focus on single-modality scenes, and overlook the complementary characteristics of tiny objects captured by multiple remote sensors. To enhance tracking performance by integrating complementary information from multiple sources, we propose a novel framework called HGT-Track (Heterogeneous Graph Transformer based Multi-Tiny-Object Tracking). Specifically, we first employ a Transformer-based encoder to embed images from different modalities. Subsequently, we utilize Heterogeneous Graph Transformer to aggregate spatial and temporal information from multiple modalities to generate detection and tracking features. Additionally, we introduce a target re-detection module (ReDet) to ensure tracklet continuity by maintaining consistency across different modalities. Furthermore, this paper introduces the first benchmark VT-Tiny-MOT (Visible-Thermal Tiny Multi-Object Tracking) for RGB-T fused multiple tiny object tracking. Extensive experiments are conducted on VT-Tiny-MOT, and the results have demonstrated the effectiveness of our method. Compared to other state-of-the-art methods, our method achieves better performance in terms of MOTA (Multiple-Object Tracking Accuracy) and ID-F1 score. The code and dataset will be made available at <https://github.com/xuqingyu26/HGTMT>.

Index Terms—Heterogeneous Graph Transformer, visible-thermal, multi-object tracking, tiny object, benchmark.

I. INTRODUCTION

MULTI-OBJECT tracking (MOT) plays a crucial role in various applications such as autonomous driving, airspace surveillance, and motion prediction [1]–[3]. With the advancement of UAV technology, drone-borne remote sensing systems have become an important tool for data collection, and served as a supplement to manned aircraft and satellite remote sensing systems. However, the detection results obtained from single-modality sensors are often unreliable in challenging situations such as low illumination, heavy occlusion, and haze [4]. To address these issues, aggregating complementary information from multiple modalities has shown promising results. Among the various sensor combinations available for drones, visible and thermal cameras are popular choices that provide high-resolution visible and thermal videos for detecting and tracking tiny objects in the far distance.

This work was supported in part by the National Natural Science Foundation of China under Grant 62301601.

Qingyu Xu, Weidong Sheng, Yingqian Wang, Chao Xiao, Chao Ma and Wei An are with the College of Electronic Science and Technology, National University of Defense Technology (NUDT), China. Emails: {xuqingyu, wangyingqian16, xiaochao12, machao0408, anwei}@nudt.edu.cn, shengweidong1111@sohu.com. (Corresponding authors: Longguang Wang; Weidong Sheng.)

Longguang Wang is with the Aviation University of Air Force, China. Email: wanglongguang15@nudt.edu.cn

Recently, several single object tracking (SOT) methods [5]–[8] have been proposed for tracking targets in visible-thermal videos, and have made significant advancements. However, the tracking of multiple tiny objects in RGB-T videos remains inadequately explored due to the following challenges:

- 1) The tracking methods that can exploit complementary information from visible and thermal modalities are mainly SOT methods, which overlook the interaction between different targets. It is non-trivial to transfer the SOT method to MOT method.
- 2) The absence of paired RGB-T video datasets hinders the progress in MOT research. While there are datasets available for object detection and single object tracking in RGB-T videos, datasets with annotated target IDs suitable for multiple tiny object tracking are still lacking.
- 3) Maintaining tiny object trajectory is challenging due to the limited detection and data association accuracy.

Although significant progress has recently been made in MOT, the leading methods can not handle the RGB-T videos well. MOT methods typically follow the tracking-by-detection (TBD) or the joint-detection-and-tracking (JDT) paradigm. The TBD methods [9]–[13] heavily rely on detection accuracy, making the tracking process susceptible to unstable detections in challenging scenarios. By using a bi-modal detector [14], [15], the TBD methods can achieve a minor improvement due to the neglect of temporal information. Some JDT techniques [16], [17] have emerged to exploit the target temporal information. However, these trackers' performance is limited in RGB-T videos as they are tailored to integrate homogeneous information and do not account for the domain gap between the visible and thermal modalities.

As illustrated in Fig. 1, the target state may differ in different modalities under diverse situations. For example, under low illumination (LI) scenarios, targets may be visible in the infrared spectrum and invisible in the visible spectrum, posing a challenge we refer to as ‘mismatch’ denoted by ‘MM’. Due to the discrepancies in target states and sensor systems, simply merging data from two modalities could hinder tracking performance.

Motivated by the success of Heterogeneous Graph Transformer in modeling web-scale heterogeneous data, we seek to use Heterogeneous Graph Transformer [18] to handle the targets discrepancies in different modalities. In this paper, we present a novel approach called HGT-Track (Heterogeneous Graph Transformer based Multi-Tiny-Object Tracking) that utilizes Heterogeneous Graph Transformer to construct the collaborative target representation. Unlike previous methods,

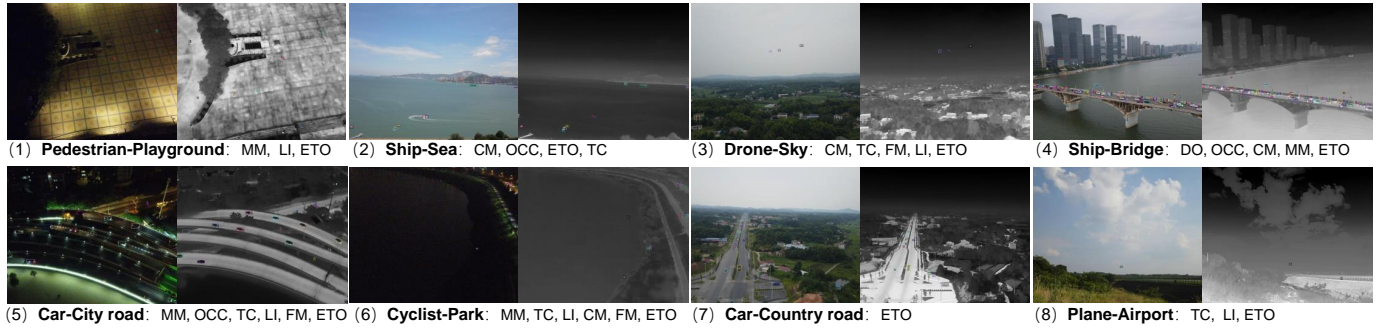


Fig. 1. Examples of 7 kinds of targets captured under 8 main scenarios in the VT-Tiny-MOT dataset are provided, along with the annotated MOT challenges (the list of challenge attributes are reported in Table II). The involved challenges are MM (MisMatch), LI (Low Illumination), ETO (Extremely Tiny Object), CM (Camera Motion), OCC (Occlusion), TC (Thermal Crossover) and FM (Fast Move).

HGT-Track models the relationship between different types of information by heterogeneous graph. Specifically, the targets at previous frame serve as tracking nodes, while the pixels at current frame serve as potential detection nodes, resulting in four types of nodes corresponding to two modalities. HGT-Track can efficiently integrate multi-modal information within the sparsely constructed heterogeneous graph. This integration allows HGT-Track to improve detection and tracking performance by leveraging the complementary information from the other modality. Notably, HGT-Track is specifically designed for multi-class small targets and is capable of recognizing objects in different scenes. Additionally, we propose a target re-detection module (ReDet) to ensure the trajectory continuity by maintaining consistency across different modalities. In addition, we develop a new visible-thermal dataset named VT-Tiny-MOT for multiple tiny object tracking. The VT-Tiny-MOT dataset includes 115 paired sequences with 1.2 million manual tracking annotations. Noted that, targets are carefully annotated separately at the visible and thermal modalities.

To summarize, our contributions are as follows:

- We propose an end-to-end Joint Detection and Tracking (JDT) framework, HGT-Track, for multiple tiny object tracking that effectively integrates visible and thermal information using Heterogeneous Graph Transformer.
- We introduce a ReDet module, which improve the trajectory continuity by maintaining consistency across different modalities.
- We construct a large-scale visible-thermal dataset named VT-Tiny-MOT for multiple tiny object tracking. Our proposed method HGT-Track achieves the best performance on thermal and visible videos of VT-Tiny-MOT as compared with other state-of-the-art trackers.

II. RELATED WORK

In this section, we briefly review three research streams that are closely related to our works.

A. Multi-modal tracking

With the increasing availability of various sensors, many multi-modal tracking methods [19]–[22] have been proposed to enhance the efficiency of tracking systems. Lukezic et al. [23] investigate the utilization of depth information in

visual object tracking. However, depth sensors are limited to a confined range of 4-5 meters. To overcome this limitation, [24] employs LiDAR and radar to capture accurate distance and angle information in autonomous driving scenarios. Compared with the sensors above, thermal sensors are more economically affordable and suitable for remote sensing applications.

RGB-T fusion tracking can be categorized into pixel-level, feature-level, and decision-level fusion, depending on when the dual-modal information is fused. Li et al. [5] propose an RGB-T fusion tracking method based on collaborative sparse representation at the decision level within a Bayesian filtering framework. To improve the efficiency of RGB-T object tracking, Zhai et al. [25] introduce a low-rank constrained tracker to perform RGB-T tracking in the correlation filter framework. Recently, several deep learning-based methods [26]–[31] have been proposed to enhance the information fusion in RGB-T tracking, which leverage the powerful capabilities of neural networks. MDNet [26] learns discriminative target representation with multiple domain-specific branches. Zhu et al. [27] propose a method to reduce the noise and redundancy after the deep aggregation of multi-modality features. Li et al. [31] propose an adaptive fusion module to improve information fusion efficiency. Though progress has been made, the deep-learning models still face problems such as large model sizes and high computation costs. Additionally, existing methods, whether traditional or deep learning-based, are all focused on single object tracking without considering target number uncertainty. Therefore, there is a necessity to explore efficient methods for multiple object tracking (MOT) in RGB-T videos.

B. Multi-object tracking

Current methods for Multiple Object Tracking (MOT) can be broadly categorized into two approaches: Tracking-by-Detection (TBD) and Joint Detection and Tracking (JDT). TBD treats tracking as a two-stage process involving detection followed by tracking. While modern detectors [32]–[34] perform well in normal scenes, accurate tracking remains challenging in remote-sensed scenes due to weak target signals. To improve tracking performance in satellite videos, Xiao et al. [11] propose DSFNet, which generates accurate detections using 3D convolution to process video clips at the cost of processing speed. Some trackers [12], [13], [35] optimize tracker

and enhance data association accuracy by carefully designed procedures. In contrast, JDT methods [36]–[39] merge the detector and tracker into a unified framework and perform joint optimization, leading to improved performance.

To capture potential high-order correlations, graph-based methods [3], [17], [39]–[41] have been proposed to exploit spatial and temporal information together. Wang et al. [17] propose a joint optimization method based on Graph Neural Networks (GNNs), which fuse spatial and temporal information to learn discriminative features. He et al. [41] introduce a graph-based spatial-temporal reasoning procedure for online target tracking in satellite videos. Additionally, offline graph-based methods [42], [43] have been proposed to improve tracking performance through global graph optimization. MP-NTrack [42] learns a neural solver to handle data association in the graph domain, while LGMTracker [43] tracks objects without appearance by encoding bounding boxes and tracklets through graph reasoning. The methods above are tailored for multiple object tracking in single modality data without considering the discrepancy between different modalities. Therefore, we extend the graph-based JDT framework for MOT in RGB-T videos by incorporating a modified Heterogeneous Graph Transformer module.

C. Small object tracking

Small object detection and tracking are challenging [44]–[46] due to low signal-to-noise ratio (SNR), particularly in military contexts, where remote objects often present as point or extended targets. Zhu et al. [46] propose MKDNet, a novel method based on a multi-level knowledge distillation network, to enhance the performance of tiny object tracking. This suggests that tiny object tracking requires additional computing resources to strengthen target features. Traditional tracking methods [47], [48] address this issue within the framework of random finite sets (RFS). RFS methods often employ techniques such as hypothesis pruning or merging to alleviate the exponentially increased computation, which can lead to a trade-off in tracking accuracy.

Inspired by the capabilities of deep learning, there have been recent efforts to simultaneously detect and track small targets. For example, CenterTrack [37] detects and tracks target as point in a unified manner. In a different approach, He et al. [41] utilize a graph-based spatiotemporal module to capture high-order relationships of small targets states between video frames in satellite videos. However, research on small target tracking using deep learning remains limited due to the lack of remote sensing data.

III. PROBLEM FORMULATION

Multiple object tracking in RGB-T videos aims at integrating complementary information from both modalities to achieve robust tracking performance.

Assume that the state of object in the visible and thermal images is denoted by a set $X_k = [X_k^v, X_k^t, q_k]$, where the superscript v and t represent the visible and thermal modality, respectively. The subscript k represents time. Since the target may be neglected by detector, the target visibility represented

by variable q may have four possibilities: sensed by both, missed by both, or sensed by one certain modality. The state vector sets X_k^v and X_k^t represent the objects state in corresponding modalities. The state vector of the i^{th} object at time k is defined as follows,

$$X_{k,i}^{v/t} = [x \quad y \quad w \quad h]^T, \quad (1)$$

where (x, y) represent the 2D position of the object in the camera image, (w, h) is the width and height of the target bounding box.

The main task is to estimate X_k with the sequence of image pairs $\{(I_i^v, I_i^t)\}_{i=1}^k$,

$$(I_0^v, I_0^t), (I_1^v, I_1^t), \dots, (I_k^v, I_k^t) \Rightarrow X_k, \quad (2)$$

where the state set at time k is estimated by processing the sequence of dual modality image pairs.

For multi-modal JDT methods, the prior for detection is provided by both modalities:

$$Prior = \text{Agg}(I_{k-1}^{v/t}, X_{k-1}^{v/t}), \quad (3)$$

where *Prior* represent the aggregated prior information to enhance object detection at time k , and function $\text{Agg}(\cdot)$ is used to integrate multi-modal information. Then, for each modality, the object can be detected with the prior information.

$$Z_k^{v/t} = \text{Det}(I_k^{v/t} | Prior), \quad (4)$$

where $\text{Det}(\cdot)$ represents the detect function, Z_k^v and Z_k^t represent the detections at time k in the visible and thermal modalities, respectively.

The tracking module takes the detection results from both modalities at time k and previous target state at time $k-1$ as input, and outputs the estimation of target state vector at time k .

$$\tilde{X}_k^{v/t} = \text{Track}(Z_k^{v/t}, I_{k-1}^{v/t}, I_k^{v/t}), \quad (5)$$

where function $\text{Track}(\cdot)$ estimates the state vector \tilde{X}_k^v and \tilde{X}_k^t . The tracking module considers both temporal information and cross-modal information to improve the accuracy of state estimation. The tracking result can be used to aid in the association of detections with tracklets. Finally, the object state X_k updates with the matched detections.

IV. METHODOLOGY

In this section, we present our HGT-Track (Heterogeneous Graph Transformer based Multi-Tiny-Object Tracking), which aims to effectively integrate spatial and temporal information from both modalities for joint online object detection and tracking. To achieve this, HGT-Track utilizes a Heterogeneous Graph Transformer (HGT) to aggregate target-specific information and enhance detection capabilities. Then, the generation of tracklets are conducted with the complementary feature. An overview of the HGT-Track framework is illustrated in Fig. 2.

We first introduce the Heterogeneous Graph Transformer-based encoder (Section IV-B). The HGT encoder fuses information by concurrently encoding four types of nodes and

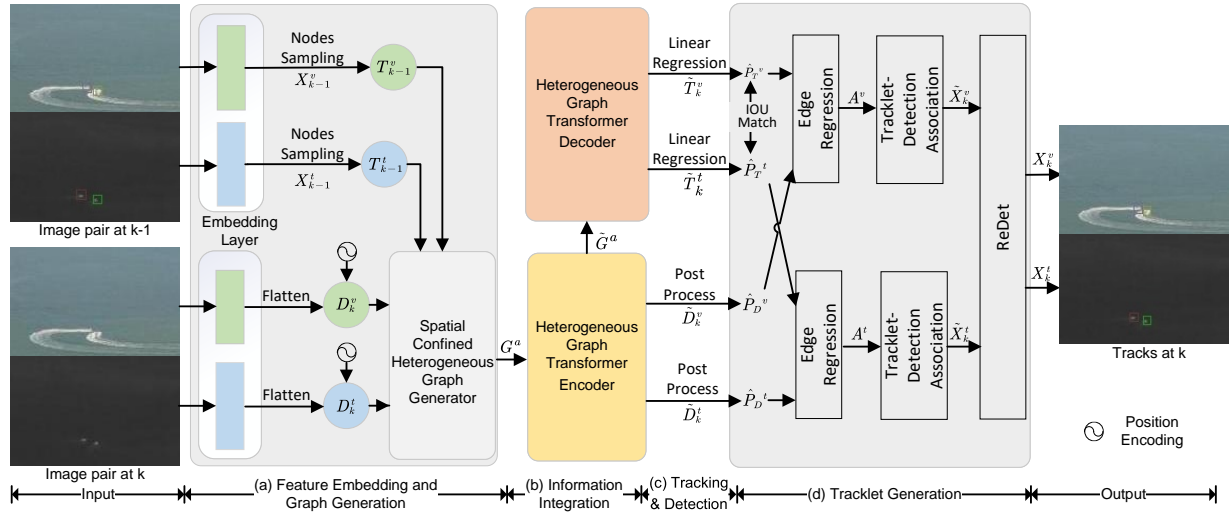


Fig. 2. The overall framework of Heterogeneous Graph Transformer based tracking method, which consists of four parts. (a) With the input of two paired visible and thermal images at time $k-1$ and k , we generate modal-specific feature through the embedding layer. Then, we build a heterogeneous graph G^a considering the target difference between two modalities. (b) Next, we utilize the modified HGT module for information integration, where the encoder output the detection feature and the decoder output the tracking feature. (c) A linear regression layer is used to generate the tracking offset, while the target detection is generated through conducting a top-k post process on detection feature. (d) Finally, tracklet is generated and further refined through cross-modal detection matching and ReDet module.

generating queries for detecting and tracking in both modalities. The dense detection queries are then used to regress and generate object detections. Subsequently, the Heterogeneous Graph Transformer decoder further decodes the sparse tracking queries to determine the tracking offset of targets in the current frame. In the tracklet generation part (Section IV-D), we introduce a ReDet module to enhance the continuity of target trajectory aided by cross-modality object matching.

A. Feature Embedding and Graph Generation

Given an RGB image $I_k^v \in \mathbb{R}^{W \times H \times 3}$ and a thermal image $I_k^t \in \mathbb{R}^{W \times H \times 1}$ obtained at time k , we initially project the images into modal-specific feature spaces using vanilla convolution. Here, W and H represent the width and height of the images, respectively. Next, we employ the parameter-shared Pyramid Vision Transformer (PVTv2) [49] to extract multiple scale features $M_k^{v/t} \in \mathbb{R}^{\frac{H}{r} \times \frac{W}{r} \times h}$ for each modality. In this context, r denotes the downscale ratio and h denotes the feature dimension. Taking each pixel as potential detection, we reshape $M_k^{v/t}$ by the operation ‘Flatten’ to generate image dense detection queries $D_k^{v/t} \in \mathbb{R}^{\frac{HW}{r^2} \times h}$ for the two modalities.

For the tracking feature, we treat the target center at previous frame as the target node. The tracking feature $T_{k-1}^{v/t} \in \mathbb{R}^{n_{k-1}^{v/t} \times h}$ are sampled from $M_{k-1}^{v/t} \in \mathbb{R}^{\frac{H}{r} \times \frac{W}{r} \times h}$, corresponding to the target nodes saved in $X_{k,i}^{v/t}$, namely ‘Nodes Sampling’. Here, n_{k-1}^v and n_{k-1}^t denote the number of targets at time $k-1$ in corresponding modalities.

The dense detection queries and sparse tracking queries serve as four types of graph nodes. Considering the bias between the two modalities, we use a heterogeneous graph G^a to model relationships among the various types of nodes. We enable sparse interactions between the two modalities on nodes connected with T_{k-1}^v and T_{k-1}^t . The spatial distance

between all the linked nodes is smaller than a threshold d . The graph G^a is defined as follows:

$$G^a = \{D_k, T_{k-1}, E_{DT}, E_{TT}, E_{DH}\}, \quad (6)$$

where D_k represents the set of potential detection nodes, T_{k-1} represents the set of tracking nodes, E_{DT} represents the sets of temporal edges that link the tracking nodes with neighboring potential detection nodes of same modalities, E_{TT} represents the sets of spatial edges that link the tracking nodes regardless of modalities, E_{DH} represents the sets of heterogeneous edges that link the tracking nodes with potential detection nodes of the other modality. These three types of edges are defined for different purposes. The temporal edges E_{DT} are used to model the association relationship between tracking nodes and detection nodes. The weight of edges E_{DT} will be further used to assign detections to target tracklets. E_{TT} focuses on analyzing the differences between targets of different modalities, which will be utilized to match objects between the two modalities. E_{DH} establishes direct links between detection nodes and tracking nodes of different modalities, and is designed to incorporate temporal information from another modality to improve the performance of object detection.

We exclude the edge connecting detection nodes from different modalities due to two reasons. **First**, fully connecting detection nodes from different modalities will result in heavy computational costs. **Second**, pixel-wise fusion is unable to suppress the influence of bias between two modalities.

B. Information Integration

The defined G^a with nodes and edges is then fed into the Heterogeneous Graph Transformer (HGT) encoder and decoder for information integration.

1) *Heterogeneous Graph Transformer encoder*: The Heterogeneous Graph Transformer encoder, as illustrated in Fig. 3 (a), is used to model the spatial and temporal correlations and

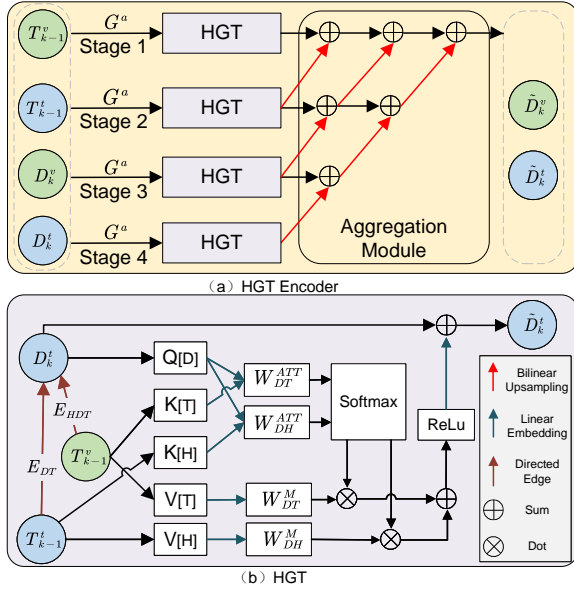


Fig. 3. The structure of the Heterogeneous Graph Transformer encoder is illustrated in (a), and the details of the Heterogeneous Graph Transformer (HGT) are shown in (b). Multi-source information is aggregated to detection queries through HGT by setting the detection queries as target nodes and other types of nodes as source nodes. Then, the information is gradually integrated into \tilde{D} from multiple stages of detection queries through the aggregation module.

learn cross-modal mapping by the modal-specific attention. Four stages of nodes D_k, T_{k-1} with the relationship defined by G^a are fed into HGT separately. Since lower feature resolution means larger receptive fields [50], we strengthen the feature of region in D_k with multi-scale features aggregated from other types of nodes linked by the directed edge E_{DT}, E_{DH} . We illustrate the mechanism of Heterogeneous Graph Transformer in Fig. 3 (b).

Traditional Transformer [51] uses a single set projections for all kinds of nodes, while in our case each kind of node connection has a distinct set of projection weight following [18]. Specifically, the distinct matrix $W_{\phi(e)}^{Att}$ and $W_{\phi(e)}^M$ are used to maintain the specific characteristics of different relations among the calculation of attention weights and message passing, where $\phi(e) \in \{DT, DH, TT\}$ denotes the type of edge. $W_{\phi(e)}^{Att}$ and $W_{\phi(e)}^M$ are optimized with the training of whole framework.

Then, we calculate the heterogeneous mutual attention between different types of nodes. For example, consider nodes D and T from the same modality. The nodes $T \in \mathbb{R}^d$ are projected through a linear layer to the i^{th} head key vector $K^i \in \mathbb{R}^{\frac{d}{h}}$, and the parameters for different heads are not shared to maximize the distribution difference. The attention is calculated by:

$$\begin{aligned} \text{Att}(D, T) &= \text{Softmax}(\text{Concat}(\text{Att}^i(Q(D), K(T))), \\ &\quad i \in [1, h]) \end{aligned} \quad (7)$$

$$\text{Att}^i(D, T) = \text{Linear}(K(T))W_{DT}^{Att}\text{Linear}(Q(D)),$$

where h is the number of attention heads, and the attention matrix is calculated by concatenating the h attention heads. The matrix $W_{DT}^{Att} \in \mathbb{R}^{\frac{d}{h} \times \frac{d}{h}}$ is distinct to capture the semantic

relations between the specific node type pairs. The attention between D and T is generated by applying softmax to all neighboring nodes to ensure that the weights sum up to 1.

The message from node T to D incorporates the edge dependency similarly by a distinct matrix W_{DT}^M :

$$\text{Message}(T) = \text{Softmax}(\text{Concat}(\text{Message}^i(K(T))), \quad (8)$$

$$\text{Message}^i(K(T)) = \text{Linear}(K(T))W_{DT}^M,$$

where the i -th message head projects source node $K(T)$ to the i -th message vector $K^i \in \mathbb{R}^{\frac{d}{h}}$. K^i is then multiplied with matrix $W_{DT}^M \in \mathbb{R}^{\frac{d}{h} \times \frac{d}{h}}$ to incorporate edge dependency. The final message passing step is to concatenate all heads messages to get $\text{Message}(T)$.

The output of HGT is then generated by using the attention weight to aggregate messages from all types of source nodes. The updated \tilde{D} is calculated as follows:

$$\tilde{D} = \sum_{\forall T \in N(D), \forall e \in E(D, T)} (\text{Att}(D, T) \cdot \text{Message}(T)), \quad (9)$$

where \sum aggregates the message from neighbor tracking nodes $N(D)$ with the attention weight.

The updated four stages of \tilde{D} are further aggregated following the Iterative Data Aggregation (IDA) method [52]. This aggregation process strengthens the detection query D by incorporating complementary information from different modalities across frames.

2) *Heterogeneous Graph Transformer decoder*: The HGT decoder, as shown in Fig. 4, is utilized to decode the tracking feature, which is subsequently used to determine the displacement of the target from the current frame to time $k-1$. The HGT incorporates multi-source information into the tracking queries \tilde{T} by setting them as target nodes. The tracking queries \tilde{T} and the current detection queries \tilde{D} are encoded with position for better spatial interaction. Finally, tracking queries \tilde{T}^v and \tilde{T}^t are learned separately through cross-deformable attention mechanism [34].

C. Object Detection and Tracking

For each modality, the decoded queries \tilde{D}_k are post processed to generate detections. First, \tilde{D}_k are reshaped back to $\mathbb{R}^{\frac{W}{r} \times \frac{W}{r} \times h}$, and then used as inputs to several branches consist of convolution layers to generate the object center heatmap $C_k \in \mathbb{R}^{\frac{W}{4} \times \frac{H}{4} \times 1}$, bounding box $S_k \in \mathbb{R}^{\frac{W}{4} \times \frac{H}{4} \times 2}$, and refine offset $R_k \in \mathbb{R}^{\frac{W}{4} \times \frac{H}{4} \times 2}$. Here, S_k contains the height and width of the object's bounding box prediction map, which has a resolution that is $\frac{1}{4}$ of the original resolution. The target center c_k are obtained by applying a threshold to C_k . The size of each object is extracted from S_k corresponding to each position c_k . The set of detections is denoted as $Z_k = \{c_{k,i}, s_{k,i}\}_{i=1}^N$.

The tracking queries \tilde{T} are input into the tracking branch, which consists of two linear layers with ReLU activation, to regress the tracking offset $t_k \in \mathbb{R}^{\tilde{N} \times 2}$, where \tilde{N} represents the number of targets at time $k-1$. Subsequently, the predicted positions of the objects $\tilde{c}_k = \{c_{k-1,i} + t_{k,i}\}_{i=1}^{\tilde{N}}$ can be computed using the predicted tracking offsets. These predicted positions are further used to assist in the detection assignment process.

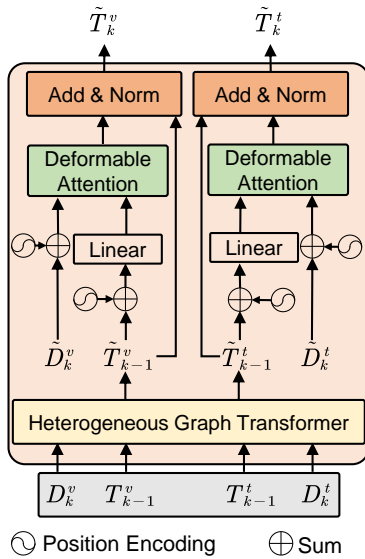


Fig. 4. Illustration of the heterogeneous transformer decoder for the generation of tracking feature \tilde{T}_k^v and \tilde{T}_k^t . Given the input of four types of nodes, namely $D_k^{v/t}$ and $T_{k-1}^{v/t}$, we set $T_{k-1}^{v/t}$ as the target node. The Heterogeneous Transformer (HGT) integrates information from $D_k^{v/t}$ to generate $\tilde{T}_{k-1}^{v/t}$. Subsequently, the tracking feature $\tilde{T}_k^{v/t}$ are generated using deformable attention strengthening.

D. Tracklet Generation

1) *Cross-modal detection matching*: Compared to normal single modality methods for MOT, HGT-Track performs cross-modal detection matching before detection-tracklet association in each modality. Given the detections Z_k^t and Z_k^v , the distance Dis between cross-modal detections is calculated using the Intersection over Union (IoU) metric:

$$Dis(i, j) = 1 - \text{IOU}(z_i^t, z_j^v), \quad (10)$$

where the function IOU computes the Intersection over Union between the i^{th} detection z_i^t in Z_k^t and the j^{th} detection z_j^v in Z_k^v . The detections are then matched using the Hungarian algorithm [53]. The variable q_k of X_k is updated based on the cross-modal matching result.

2) *Detection and tracklet association*: Then, we assign the detections to existing tracklets based on the edge affinity matrix A . The edge weights of A are determined through regression using the edge feature. Specifically, the detection feature $U \in \mathbb{R}^{N \times h}$ is sampled from $\tilde{D}_k \in \mathbb{R}^{\frac{W \times H}{r^2} \times h}$ at the corresponding detection positions. On the other hand, the tracking feature $V \in \mathbb{R}^{N \times h}$ corresponds to \tilde{T} exactly. The edge feature E is defined as:

$$E_{ij} = U_i - V_j, \quad (11)$$

where U_i is the feature of the object at the i^{th} detection node and V_j is the feature of the j^{th} tracking node. The affinity matrix A of dimension $N \times N \times 1$ is then regressed from E .

$$A = \text{Sigmoid}(\text{Conv2}(\text{ReLU}(\text{Conv1}(E))))), \quad (12)$$

where Conv1 and Conv2 represent two convolutional layers with a kernel size of 1, and Sigmoid function is used to output the values of A between 0 and 1. The matrix A can be used

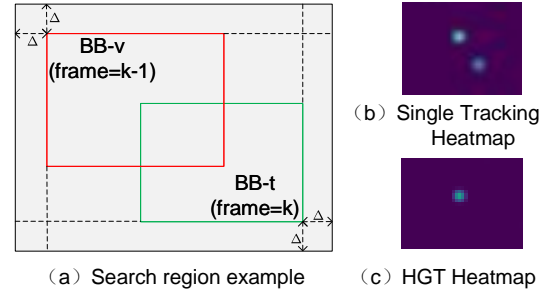


Fig. 5. An example of the region area to re-detect the lost target. If the target is lost by the visible camera but can still be detected by the thermal camera, we initiate a re-detection procedure within a search region SR colored by gray at time k , as depicted in (a). This search region encompasses the union area of the target's bounding box at time $k-1$ in the visible camera and time k in the thermal camera. In (b), we present the heatmap generated using ReDet to locate the lost target. Comparing it with the original HGT detection heatmap shown in (c), we can observe that even in a close-proximity scenario, another target can be accurately detected in the single tracking heatmap.

to associate the detected objects with existing tracklets using the Hungarian algorithm [53]. If a newly detected object can be detected at 3 consecutive frames, it will initialize a new tracklet. Tracklets will be ended if they are lost for more than 20 frames.

3) *Re-detect target*: The target is likely to have similar cross-modal tracklets if it can be detected by both modalities. In cases where no detection matches with target $X_{k-1,i}^v$, we attempt to re-detect the target $X_{k,i}^v$ within the search region SR of the visible frame, as illustrated in Fig. 5, but only if X_i has been detected in both modalities. The search region is slightly larger than the union region of the bounding box of $X_{k-1,i}^v$ and $X_{k,i}^t$. Since target $X_{k,i}^v$ is too dim to be directly detected, we leverage the prior information from the other modality to provide complementary information. Specifically, we utilize the hybrid target feature output from the HGT encoder to correlate with the search feature extracted from \tilde{D}_k^v corresponding to the search region, similar to single object tracking. The pixels within the search region are treated as nodes representing potential detections, and the affinity matrix is computed following Eq. 12, which serves as the correlation score map. The position with the highest score is further checked using our proposed two principles. The first principle checks whether the IOU distance between the re-detected target $X_{k-1,i}^v$ and $X_{k,i}^v$ exceeds a certain threshold. The second principle checks whether the detection score is above a filtered threshold \tilde{Det} :

$$\tilde{Det} = \frac{Det}{1 + c_{k,i}^h}, \quad (13)$$

where $c_{k,i}^h$ represents the detection score of the lost target in the other modality, and Det represents the detection threshold of the detector. Consequently, the position of re-detected target is computed as:

$$(x, y) = \arg \max(A(E_{SR})), \quad (14)$$

$$\text{if } C_k(x, y) > \tilde{Det}, \text{IOU}(Z_{k,i}, Z_{k-1,i}) > \tau,$$

where E_{SR} represents the edge matrix between the lost target feature and the search feature, and τ is a selected threshold.

Algorithm 1 The pipeline of Tracklet Generation

Input: Detections Z_k , object state X_{k-1} ;

- 1: Match the detections in both modalities Z_k^v and Z_k^t depending on IOU distance;
- 2: **for** each modality **do**
- 3: Assign detections Z_k to object X_{k-1} using affinity matrix A .
- 4: Update object state if it is matched with a detection.
- 5: Get the lost objects LT if it is unmatched;
- 6: **for all** $lt \in LT$ **do**
- 7: **if** $X_{k-1,lt}$ is updated in one modality at step 4 **then**
- 8: Re-detect $X_{k,lt}$ at the search region SR using Eq.14;
- 9: **end if**
- 10: Update $X_{k,lt}$;
- 11: **end for**
- 12: **end for**

Output: X_k^v and X_k^t ;

The details of the tracklet generation are summarized in Algorithm 1.

E. Loss Function

The loss function consists of a detection loss term and a data matching loss term.

1) *Detection Loss:* The detection loss is composed of 4 parts including the center focal loss L_{cf} , the box size loss L_{bs} , the refinement loss L_r and the tracking displacement loss L_{td} . The aforementioned four loss terms correspond to the classification branch and three regression branches, respectively.

The center focal loss [54], [55] L_{cf} is used to train the heat map branch, which simultaneously penalize the classification error and localization error. The ground-truth heatmap $Y \in [0, 1]^{\frac{H}{4} \times \frac{W}{4} \times 7}$, where 7 is the number of object classes. L_{cf} is composed of the center focal loss L_{cf}^t and L_{cf}^v in two modalities, and L_{cf}^v is computed as follows,

$$L_{cf}^v = \frac{1}{N^v} \sum_{xyc} \begin{cases} (1 - \hat{Y}_{xyc})^\alpha \log(\hat{Y}_{xyc}) & \text{if } Y_{xyc} = 1 \\ (1 - Y_{xyc})^\beta (\hat{Y}_{xyc})^\alpha \log(1 - \hat{Y}_{xyc}) & \text{otherwise} \end{cases}, \quad (15)$$

Loss L_{cf}^t is computed similarly to L_{cf}^v .

For the remaining branches, losses are computed sparsely at the position of targets, i.e. the i^{th} object at location \mathbf{p}_i with the bounding box size s_i , the loss is computed as follows:

$$L_{bs} = \frac{1}{N^v} \sum_{i=1}^{N^v} |\hat{S}_{\mathbf{p}_i}^v - s_i^v| + \frac{1}{N^t} \sum_{i=1}^{N^t} |\hat{S}_{\mathbf{p}_i}^t - s_i^t|, \quad (16)$$

Analogously to L_{bs} , the refinement loss L_r and the tracking displacement loss L_{td} are also computed at the center position of targets. The overall detection loss is the weighted sum of the four loss items.

2) *Data matching loss:* In the detection and tracklet association part, the affinity matrix A is regressed from the edge feature E . In the training stage, the target tracking nodes $\{\hat{T}_{k,i}\}_{i=1}^N$ and the N detection nodes are sampled from \bar{D} with the groundtruth positions. The edge feature E as Equation 11 for the regression of A .

The data matching loss L_{match} is used to encourage matrix A to approach an identity matrix $I \in \mathbb{R}^{N \times N}$. L_{match} is formulated as the combination of the binary cross entropy loss L_{BCE} and the cross entropy loss L_{CE} .

The loss L_{BCE} is computed pixel-wisely on A to supervise the binary classification problem of the edges. It encourages A to be close to either 0 or 1. The loss L_{CE} is computed to encourage each row and column of A to be a one-hot vector.

$$L_{match} = \sum_{i \in \{t,v\}} L_{BCE}^i + L_{CE}^i,$$

$$L_{BCE} = -\frac{1}{N^2} \sum_{i=1}^N \sum_{j=1}^N I_{ij} \log(A_{ij}) + (1 - A_{ij}) \log(1 - A_{ij}),$$

$$L_{CE} = -\frac{1}{N} \sum_{i=1}^N A_{ij} \log\left(\frac{e^{A_{ij}}}{\sum_{i=1}^N e^{A_{ij}}}\right) - \frac{1}{N} \sum_{j=1}^N A_{ij} \log\left(\frac{e^{A_{ij}}}{\sum_{j=1}^N e^{A_{ij}}}\right), \quad (17)$$

where N is the number of targets that simultaneously appear in one modality. L_{match} represents the loss values from two modalities. L_{CE} is computed per row and column.

V. VISIBLE-THERMAL TINY MULTIPLE OBJECT TRACKING BENCHMARK

In this section, we introduce the newly collected visible-thermal tiny multiple object tracking (VT-Tiny-MOT) benchmark, including dataset construction with statistics analysis and baseline methods with both single-modality and dual-modality inputs.

A. Data Collection and Annotations

The visible and thermal videos were simultaneously recorded using visible and thermal cameras mounted on a professional UAV (DJI Mavic 2). Each video pair consists of a visible video and a thermal video. To ensure accurate alignment between the two modalities, a homography matrix is computed using Zhang’s method [56] and applied to align the remaining frames of each video pair. However, due to two main factors, the registration accuracy is limited, and there exists bias between each video pairs.

First, the vertical arrangement of the cameras on the UAV leads to variations in the depth of field (Dof), which violates the assumptions made in [56]. **Second**, the Zhang’s method [56] is ineffective in handling the disparity variations in stereo image pairs [57], especially in cases of texture-lacking images. Despite these limitations, the dataset has been refined to achieve a frame rate of 15 FPS and a resolution of 512×640 pixels.

To capture diverse scenarios, the video pairs in our dataset were recorded in eight distinct outdoor scenes: sea, lake, bridge, city road, country road, playground, airport, and sky, under different seasons, weathers, and illuminations. The recording UAV was operated in three different states: cruise, hover, and ground. Each state determined the height and motion style of the camera. Further details regarding the challenges posed by these scenarios will be discussed in Section V-B.

Ground truth annotations for objects in the visible and thermal modalities are provided separately in our dataset. The annotations include the location, category, and tracking ID of each object, following the label format specified by the MOT challenge [58]. The visible and thermal annotations are paired with a one-to-one correspondence, except for extreme conditions such as low illumination. The tracking IDs are consistent across different modalities, enabling comprehensive evaluation of tracking methods. To ensure the quality of the data annotations, professional annotators were employed, and a thorough verification process was conducted. The annotations undergo frame-by-frame evaluation by a minimum of three assessors to minimize errors and inconsistencies.

B. Statistics

The VT-Tiny-MOT dataset comprises a total of 115 video pairs, capturing a diverse range of circumstances, as illustrated in Fig. 1. The dataset contains 5208 instances of objects across seven different categories: ship, pedestrian, cyclist, car, bus, drone, and plane. The scene distribution and relevant target distribution with average numbers per frame are illustrated in Fig. 6 (a). The target type is highly correlated with the scene category (ship accounts for 97% in ‘Sea’ scene and car accounts for 73% in ‘Cityroad’ scene). Due to variations in target states across modalities, targets were annotated separately for each modality, and the target distribution for each modality is depicted in Fig. 6 (b).

To provide a context for the dataset, we compare its statistics with other RGB-T (visible-thermal) and small object tracking (SOT) datasets, as presented in Table I. This comparison allows researchers to understand the uniqueness and characteristics of the VT-Tiny-MOT dataset as compared to existing datasets.

Additionally, we identify ten specific challenges in the dataset, which are detailed in Table II. These challenges encompass various factors such as occlusion, low illumination, camera motion and others, which pose difficulties for object tracking algorithms. We analyze the dataset from the following aspects.

1) *Small object*: The presence of small targets poses a significant challenge due to their limited size and lack of rich shape and texture information. Compared to normal-sized objects, small targets are more difficult to perceive and track accurately. Specifically, the objects in the VT-Tiny-MOT dataset are mainly small targets, following the definition in [59]. As show in Table II, there are over 95.83% of the targets being smaller than 1024 pixels.

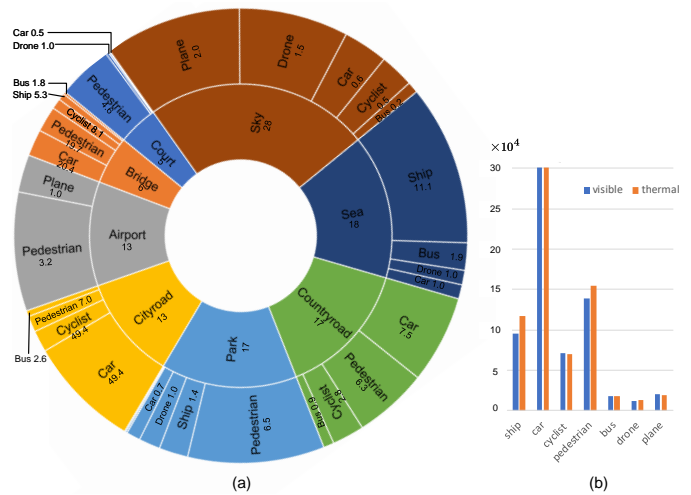


Fig. 6. Statistics of the VT-Tiny-MOT dataset. (a) Distribution of scene (inner) with sequence numbers annotated and object category (outer) with average target number per frame annotated. (b) The target distribution in each modality.

2) *Occlusion*: Occlusion occurs when targets are partially or fully obscured by the environment or other targets. For example, targets on city roads may be occluded by trees or buildings. Additionally, group targets such as helicopters can occlude each other. It is important to note that occlusion can also occur asymmetrically between the two modalities. In other words, a target may be occluded in one modality while still visible in the other modality. This introduces additional challenges for tracking algorithms, as they need to handle occlusion scenarios and effectively utilize the available modalities to maintain accurate object tracking.

3) *Modality mismatch*: Due to the possibility of target loss in one modality, the annotations of a target in the two modalities do not always have an exact one-to-one correspondence. Modality mismatch, as a challenge, is closely related to two specific challenges, Low Illumination (LI) and Thermal Crossover. In scenarios with low illumination, targets are difficult to detect by the visible camera, but the thermal information can aid in perceiving the targets. When an object has a similar temperature to the background, integrating the object information from the visible camera becomes useful in discriminating the object from the background. Despite the modality mismatch challenge, the overall quantities of visible and thermal annotations are comparable.

C. Baseline Methods

For evaluating the proposed method HGT-Track and providing a comprehensive evaluation benchmark, we include some popular tracking methods as baselines into our VT-Tiny-MOT benchmark.

On one hand, there are 11 state-of-the-art single-modality trackers presented to demonstrate their performance in challenging scenarios, including DeepSORT [9], Tractor [10], ByteTrack [12], OCSORT [13], DSFNet [11], MPNTrack [42], CenterTrack [37], FairMOT [38], TransCenter [63], TraDes [64] and GSDT [17]. On the other hand, we also

TABLE I

STATISTIC COMPARISON AMONG EXISTING RGB-T AND SMALL OBJECT TRACKING (SOT) DATASETS. ‘‘CAT’’ REPRESENTS THE NUMBER OF TARGET CATEGORIES. ‘‘SMALL TARGET’’ AND ‘‘MULTI TARGETS’’ REPRESENT WHETHER THE CAPTURED TARGETS OF THE DATASET ARE SMALL AND MULTIPLE, RESPECTIVELY.

Benchmark	Booketitle	Year	Platform Frames	Seq.	Total Frames	Anno.	Resolution	Target Caotegories	Small	Multiple
GTOT [5]	TIP	2016	Ground	50	7.8K	7.8K	384 × 288	4	×	×
VOT-RGBT [60]	ICCVW	2019	Ground	60	40K	40K	630 × 460	13	×	×
RGBT234 [61]	PR	2019	Ground	234	233.8K	233.8K	630 × 460	22	×	×
LasHeR [62]	TIP	2021	Ground	1224	6.7M	6.7M	630 × 480	32	×	×
Anti-UAV [45]	TPAMI	2021	Ground	318	7.8K	7.8K	640 × 512	1	✓	×
VTUAV [8]	CVPR	2022	UAV	500	3.3M	326K	1920 × 1080	13	✓	×
VT-Tiny-MOT(ours)	-	-	UAV	115	93K	1.2M	512 × 640	7	✓	✓

TABLE II

LIST OF THE ATTRIBUTES ANNOTATED TO THE DATASET VT-TINY-MOT. WE ALSO REPORT THE NUMBERS OF THE SEQUENCES AND ANNOTATIONS IN VT-TINY-MOT CONCERNING THE CORRESPONDING CHALLENGE AT THE ‘SEQ’ COLUMN AND THE ‘ANNS’ COLUMN, RESPECTIVELY.

Modality	Attribute	Full Name	Seq	Anns	Description
RGB	OCC	Occlusion	36	0.1M	The target is partially or fully occluded.
	ETO	Extremely Tiny Object	105	0.45M	The number of pixels in the ground truth bounding box is less than 64.
	TO	Tiny Object	110	0.51M	The number of pixels in the ground truth bounding box is between 64 and 256.
	SO	Small Object	71	0.19M	The number of pixels in the ground truth bounding box is between 256 and 1024.
	DO	Dense Object	10	0.32M	Targets densely appear in a region.
	LI	Low Illumination	55	0.16M	The illumination in the target region is low.
	FM	Fast Move	63	0.01M	Targets move beyond 10 pixels between two consecutive frames.
	MM	Mismatch	92	0.13M	Targets do not appear simultaneously in both modalities.
CM	Camera Motion	17	365	Camera moves when capturing the video.	
Thermal	TC	Thermal Crossover	55	0.16M	The target has similar temperature with other objects or background.

implement 3 visible-thermal trackers by integrating bi-modal detectors ProbEn [14] and UA-CMDet [15] within DeepSORT, referred to as ‘ProbEn-E+SORT’, ‘ProbEn-M+SORT’, and ‘UA-CMDet+SORT’, where ‘ProbEn-E’ indicates the early fusion version of ProbEn, and ‘ProbEn-M’ denotes the middle fusion version. Note that, Faster R-CNN [65] is utilized as the detector in TBD methods [9], [10], [12], [13], [42]. For the JDT methods [17], [37], [38], [63], [64], training and testing are conducted following the protocols outlined in the respective original papers. The methods above are trained with various modalities, which is indicated in column ‘Mod’.

VI. EXPERIMENTS

In this section, we present a comprehensive evaluation of the proposed cross-modal tracking method on the VT-Tiny-MOT dataset. We first present details about the implementation of our method. Subsequently, we conduct ablation study to analyze the effectiveness of different components of our proposed method. Finally, we compare our method with other state-of-the-art tracking methods.

A. Implementation Details

1) *Evaluation metrics*: To evaluate the performance of multi-object trackers in RGBT videos on the VT-Tiny-MOT benchmark, we employ several common quantitative metrics. These metrics provide insights into various aspects of tracking performance. The metrics used for evaluation include Higher-Order Tracking Accuracy (HOTA), Multi-Object Tracking Accuracy (MOTA), Multi-Object Tracking Precision (MOTP), ID-F1 Score (IDF1), ID switch (IDs), Mostly tracked targets

(MT), Mostly lost targets (ML), False Positive (FP), and False Negative (FN). MOTA, MOTP, and IDF1 are employed to assess the overall performance of each tracker, while IDs, MT, ML, FP, and FN are reported to facilitate further comparison among the trackers. The symbol \uparrow after the metric means higher is better, while \downarrow means lower is better. To ensure a more effective evaluation, considering the small size of the targets, we set the Intersection over Union (IOU) threshold to 0.3.

2) *Experimental Settings*: In the experiment, we utilized the PVTv2 as the embedding layer and employed the pretrained model to expedite the convergence of HGT-Track training. We computed the loss separately for each modality, and the sum of the losses was backpropagated to update the network parameters. The downscale ratio of the image feature was set to 4 to enable training on limited GPU computing resources. The detection threshold for both modalities was set to 0.4. All experiments were conducted on an RTX 3090 GPU. We set the graph layer to 1 and the spatial radius to 20. The training converged at around 20 epochs.

B. Ablation Study

1) *Heterogeneous Graph Transformer*: To evaluate the effectiveness of our Heterogeneous Graph Transformer (HGT) information integration module, we conducted experiments by training our model using varying numbers of HGT layers in the HGT encoder, denoted as ‘l-layer HGT’, where ‘l’ represents the number of HGT layers. The evaluation results for the visible and thermal test sequences are presented in

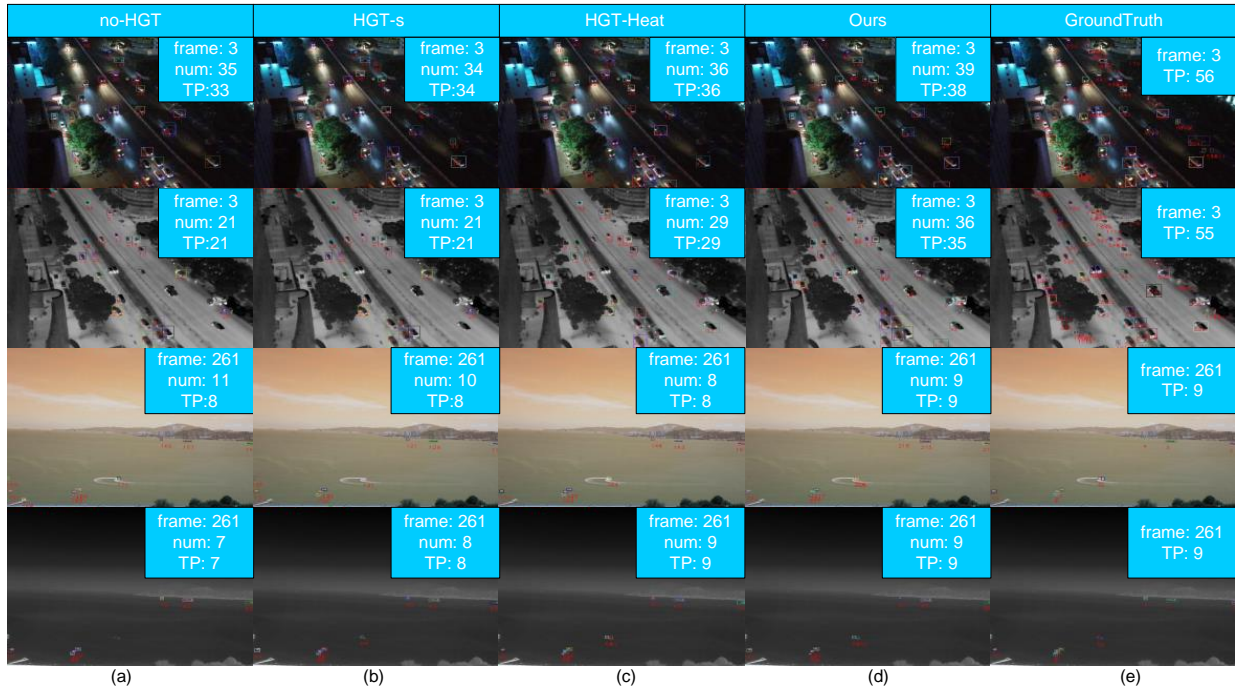


Fig. 7. Qualitative results of our proposed method with different settings on two selected sequence pairs, namely "Night Street" (upper two rows) and "Afternoon Sea" (bottom two rows), from the test set of VT-Tiny-MOT. The columns (a)-(d) display the results of different trackers. Our proposed tracker can generate more robust tracking results under such challenging scenarios.

Table III. Additionally, we trained a variant tracker without HGT, referred to as no-HGT.

Our HGT-based model consistently outperformed the variant 'no-HGT' across most evaluation metrics. Specifically, compared to 'no-HGT', '1-layer HGT' demonstrated an improvement of 6.7/4.1% at MOTA on the visible/thermal test sequences, respectively. Furthermore, the identification probability assessed by IDF1 exhibited enhancements of 12.4/10.2% in both modalities. With the number of HGT layer increases, the performance of '1-layer HGT' consistently surpasses 'no-HGT', demonstrating the effectiveness of HGT.

2) *Multi-Modal information integration*: To demonstrate the effectiveness of multi-modal information integration, we introduced the variant '1-layer HGT-s' that solely relies on single modality information by excluding the edges DH in '1-layer HGT'. As shown in Table III, the '3-layer HGT-s' variant exhibited an enhancement of 0.5/2.4% at MOTA on the visible and thermal test sequences, respectively, compared to 'no-HGT'. This improvement demonstrates the effectiveness of incorporating temporal information. Furthermore, '1-layer HGT' showed superior performance to '1-layer HGT-s' across different numbers of HGT layers, which demonstrates the effectiveness of HGT in integrating information from visible and thermal modalities.

3) *ReDet*: The ReDet module is proposed to promote consistency of object states between the two modalities. We compare our tracker with the variant without ReDet module ('Ours w/o ReDet') and another variant that utilizes heatmap-based re-detection, denoted as 'HGT-Heat'. 'HGT-Heat' performs re-detection of lost targets by employing the heatmap associated with the search region SR .

The tracking performance is reported in Table IV. 'Ours

w/o ReDet' achieves the lowest false positive (FP) rate due to a trade-off between FP and FN since neither of the re-detection methods can fully recognize the true target. 'HGT-Heat' exhibits poor performance with -0.05% in MOTA, due to a significant increase in false positives resulting from the lack of identity information in the heatmap. In contrast, 'Ours w/ ReDet' effectively re-detects the lost targets using the correlation score map followed by the verification of target. This results in an improvement of 4.3% in MOTA and 9.8% in IDF1 as compared to 'Ours w/o ReDet', demonstrating the effectiveness of ReDet module.

Furthermore, we illustrate the results obtained by 'Ours w/ ReDet' under two distinct scenarios in column (d) of Fig. 7. In the sequence pair "Afternoon Sea", two ships are occluded by splashing water in the visible modality, while they are accurately recognized in the thermal modality. Our proposed tracker successfully re-detect the lost target in visible modality through the ReDet module, addressing the occlusion challenge.

4) *The classification branch*: In the context of detection methods, the classification branch is commonly used to increase the inter-class difference between objects and decrease the intra-class difference. HGT-Track leverages the detection features as the ReID features of the target to associate targets across different time steps.

To explore the effectiveness of classification branch within the remote sensing domain, we trained the detector using a binary classification network that was specifically designed to discriminate the target from background. This particular variant is referred to as 'Single'. The detailed tracking results are listed in Table VI. A comparison with the tracking results obtained by the single-class model 'Single' reveals that HGT-Track achieved an improvement of 2.4/2.6% in terms of

TABLE III

ABLATION STUDY ON THE EFFECTIVENESS OF HGT AND MULTI-MODAL INFORMATION INTEGRATION. QUANTITATIVE RESULTS ON THE ‘VISIBLE’ AND ‘THERMAL’ TESTING SEQUENCES OF THE DATASET VT-TINY-MOT ARE DISPLAYED, WITH THE TOP RESULTS HIGHLIGHTED IN BOLD. THE COLUMN TI REPRESENT THE USAGE OF TEMPORAL INFORMATION.

	Method	Mod	TI	HOTA↑	MOTA↑	MOTP↑	MT↑	ML ↓	FP↓	FN ↓	IDF1↑	IDs↓
Visible	no-HGT	V	✗	22.8	25.3	54.2	125	459	13669	117576	30.8	2972
	1-layer HGT-s	V	✓	24.9	27.2	55.0	156	430	16860	110652	33.6	3375
	2-layer HGT-s	V	✓	23.5	24.0	55.1	140	429	20459	112799	31.9	3334
	3-layer HGT-s	V	✓	24.7	25.8	55.2	153	421	19025	111115	34.6	3277
	4-layer HGT-s	V	✓	20.1	14.7	59.9	86	624	6977	144523	21.5	1914
	1-layer HGT	V+T	✓	29.1	32.0	55.6	226	444	11594	109500	43.2	1223
	2-layer HGT	V+T	✓	29.4	31.6	55.2	268	406	16787	104812	43.7	1288
	3-layer HGT	V+T	✓	29.4	32.1	55.1	257	399	15595	105060	43.8	1379
4-layer HGT	V+T	✓	28.9	29.5	55.9	211	422	13835	111826	41.2	1053	
Thermal	no-HGT	T	✗	18.3	17.2	52.1	60	641	8395	146650	25.1	1252
	1-layer HGT-s	T	✓	18.3	14.5	50.9	66	618	13307	146580	24.9	1348
	2-layer HGT-s	T	✓	18.3	17.4	50.2	72	618	10632	143687	25.9	1496
	3-layer HGT-s	T	✓	20.5	19.6	53.1	90	594	11162	138768	29.1	1736
	4-layer HGT-s	T	✓	14.0	8.1	53.8	35	742	5330	167064	13.8	1048
	1-layer HGT	V+T	✓	23.1	21.3	51.5	155	588	12516	135197	35.3	844
	2-layer HGT	V+T	✓	21.3	16.6	49.6	87	606	14913	141765	31.0	605
	3-layer HGT	V+T	✓	22.3	19.1	50.7	103	574	16928	134726	33.0	997
4-layer HGT	V+T	✓	24.8	22.1	50.9	159	556	15695	130493	33.7	725	

TABLE IV

ABLATION STUDIES ON THE EFFECTIVENESS OF ReDet MODULE. QUANTITATIVE RESULTS ON THE ‘VISIBLE’ AND ‘THERMAL’ TESTING SEQUENCES OF THE DATASET VT-TINY-MOT ARE DISPLAYED, WITH THE TOP RESULTS HIGHLIGHTED IN BOLD.

	Method	HOTA↑	MOTA↑	MOTP↑	MT↑	ML ↓	FP↓	FN ↓	IDF1↑	IDs↓
Visible	Ours w/o ReDet	24.8	27.7	55.7	134	485	9082	118231	33.4	2749
	HGT-Heat	28.5	-5.4	54.5	267	386	69898	99332	17.5	20334
	Ours w/ ReDet	29.1	32.0	55.6	226	444	11594	109500	43.2	1233
Thermal	Ours w/o ReDet	20.3	19.8	51.9	88	614	9468	140232	28.8	1492
	HGT-Heat	15.3	-10.7	50.5	180	497	72355	121539	18.5	14945
	Ours w/ ReDet	23.1	21.3	51.5	155	588	12516	135197	35.3	844

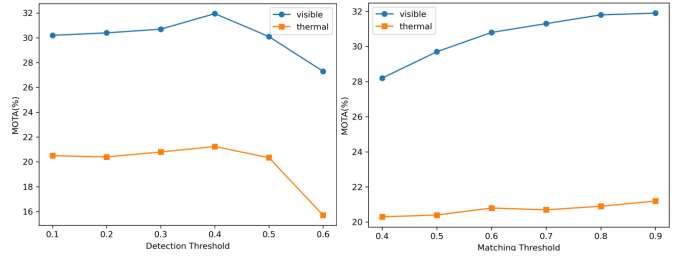


Fig. 8. Illustration of the influence of the detection threshold \tilde{D}_{det} and matching threshold τ .

MOTA for the visible and thermal modalities, respectively. These improvements effectively demonstrate the contribution of multi-classification branch to the overall performance of the proposed tracker.

C. Discussion

1) *Detection and matching threshold:* In the ReDet module, we propose two principles for checking the target position before tracklet generation. Lowering the detection threshold \tilde{D}_{det} allows for the detection of more targets with low confidence, but it also increases the number of false alarms. On the other hand, a higher \tilde{D}_{det} would decrease the number of true positives. The impact of the detection threshold on tracking performance is illustrated in Fig. 8. While having more tracking nodes may facilitate better information aggregation from the other modality, it does not necessarily lead to improved tracking performance. Our sparse information fusion approach relies on accurate detection results, and increasing the number of false alarms degrades the overall tracking performance.

As for the IOU matching threshold τ , a lower τ indicates a higher tolerance for differences in target detection between the two modalities. With an increase in τ , there is a steady improvement in tracking performance in both modalities. This reflects that VT-Tiny-MOT is aligned at the pixel level, and

a higher IOU matching threshold will eliminate false alarms generated with the guidance of information from the other modality in the ReDet module.

2) *Limitations:* In our proposed method, we track the target and maintain the tracklet by leveraging information from both modalities at the feature and decision levels. Through the designed HGT information fusion module, we are able to effectively reduce false positives and false negatives. However, at a later stage, we prioritize maintaining the completeness of the tracklet, which may lead to a slight increase in false positives. This can be attributed to the heuristic setting of the ReDet module, which refines the target based on the physical prior that the tracklet should exhibit consistency in both modalities. However, false alarms are also retained under this setting.

D. Comparison with Other Trackers

In Table V, we present a comprehensive comparison of HGT-Track with other state-of-the-art trackers using the test set of VT-Tiny-MOT. Our proposed tracker outperforms all currently dominant trackers in terms of overall performance, achieving the highest MOTA and IDF1 in both modalities. For instance, compared to the ByteTrack tracker, HGT-Track shows an improvement of 13/2.6% higher MOTA and

TABLE V

QUANTITATIVE RESULTS ON THE ‘VISIBLE’ AND ‘THERMAL’ TESTING SEQUENCES OF THE DATASET VT-TINY-MOT ARE DISPLAYED, WITH THE TOP AND SECOND-TOP RESULTS HIGHLIGHTED IN RED AND BOLD, RESPECTIVELY. THE GNN-BASED TRACKING METHODS MARKED WITH AN ASTERISK (*) HAVE BEEN MODIFIED AND RETRAINED BEFORE EVALUATED ON THE VT-TINY-MOT DATASET.

	Methods	FW	Mod	Backbone	HOTA ↑	MOTA ↑	MOTP ↑	MT ↑	ML ↓	FP ↓	FN ↓	IDF1 ↑	IDs ↓	FPS ↑	Params ↓
Visible	DeepSORT [9]	TBD	V	ResNet50	23.4	12.4	68.8	15	623	7043	148453	20.7	2062	28.8	41.3
	Tracktor [10]	TBD	V	ResNet50	23.3	3.0	64.2	152	605	28494	144647	22.5	1283	10.6	67.2
	ByteTrack [12]	TBD	V	ResNet50	26.3	13.3	68.7	152	625	6670	148259	26.3	844	38.4	41.3
	OCSORT [13]	TBD	V	ResNet50	25.8	10.6	68.0	156	612	11940	146690	25.7	2034	24.3	41.3
	MPNTrack * [42]	TBD	V	ResNet50	23.0	3.5	62.4	168	594	29528	143452	24.6	418	-	21.0
	DSFNet [11]	TBD	V	DLA34	16.3	10.4	64.3	32	747	911	159954	16.6	290	10.5	17.0
	CenterTrack [37]	JDT	V	DLA34	11.8	10.3	71.6	16	680	1859	154977	8.8	3933	41.0	19.7
	FairMOT [38]	JDT	V	DLA34	22.7	12.1	67.6	76	688	2721	153421	22.4	1960	21.7	20.1
	TraDes [64]	JDT	V	DLA34	20.0	8.8	66.0	82	691	9938	153532	20.4	428	30.3	20.9
	GSDT * [17]	JDT	V	DLA34	22.7	8.9	71.3	76	688	2722	153415	22.4	1950	1.3	21.0
	Transcenter [63]	JDT	V	PVTv2	5.0	-4.0	46.6	11	856	10522	176028	2.1	349	22.3	35.0
	HGT-Track-V (Ours)	JDT	V	PVTv2	23.1	27.2	55.0	156	430	16860	110652	33.6	3375	15.2	30.7
	ProbEn-E+SORT [14]	TBD	V+T	ResNet50	20.0	9.5	66.7	138	542	19024	134952	17.4	8758	-	60.3
	ProbEn-M+SORT [14]	TBD	V+T	ResNet50	26.3	24.7	67.4	211	450	12108	111365	26.1	11930	-	120.6
UA-CMDet+SORT [15]	TBD	V+T	ResNet50	24.1	8.6	65.1	190	464	36612	121063	23.2	6696	-	139.2	
HGT-Track (Ours)	JDT	V+T	PVTv2	29.1	32.0	55.6	226	444	11594	109500	43.2	1223	13.2	30.7	
Thermal	DeepSORT [9]	TBD	T	ResNet50	21.9	8.4	73.7	142	689	9859	160768	17.2	2158	28.7	41.3
	Tracktor [10]	TBD	T	ResNet50	24.5	5.8	69.5	153	661	22465	154425	2.7	881	11.6	67.2
	ByteTrack [12]	TBD	T	ResNet50	25.5	9.2	73.9	150	692	9835	160458	22.6	915	34.1	41.3
	OCSORT [13]	TBD	T	ResNet50	24.4	0.9	71.6	153	655	27143	156803	21.4	2921	17.5	41.3
	MPNTrack * [42]	TBD	T	ResNet50	18.8	-9.1	62.8	152	635	53635	151498	19.0	847	-	21.0
	DSFNet [11]	TBD	T	DLA34	20.5	13.7	65.3	42	758	3678	158828	23.6	307	10.2	17.0
	CenterTrack [37]	JDT	T	DLA34	15.0	18.8	72.2	53	591	3089	143279	13.3	6194	39.9	19.7
	FairMOT [38]	JDT	T	DLA34	15.3	8.0	62.2	45	785	1676	170889	14.9	928	19.8	20.1
	TraDes [64]	JDT	T	DLA34	26.0	15.7	67.0	153	609	15271	143153	30.5	532	28.3	20.9
	GSDT * [17]	JDT	T	DLA34	15.3	8.9	62.3	45	785	1678	170891	14.9	927	0.9	21.0
	Transcenter [63]	JDT	T	PVTv2	4.8	0.2	62.3	2	909	1628	186443	1.6	129	22.5	35.0
	HGT-Track-T (Ours)	JDT	T	PVTv2	18.3	14.5	50.9	66	618	13307	146580	24.9	1348	15.2	30.7
	ProbEn-E+SORT [14]	TBD	V+T	ResNet50	19.3	14.0	69.8	126	630	10229	144052	17.0	7981	-	60.3
	ProbEn-M+SORT [14]	TBD	V+T	ResNet50	20.7	18.3	70.4	250	428	9649	110327	16.3	34042	-	120.6
UA-CMDet+SORT [15]	TBD	V+T	ResNet50	19.8	10.5	66.6	247	466	24452	120005	15.6	24390	-	139.2	
HGT-Track (Ours)	JDT	V+T	PVTv2	23.1	21.3	51.5	155	588	12516	135197	35.3	844	13.2	30.7	

TABLE VI

ABLATION STUDIES ON THE EFFECTIVENESS OF MULTI-CALSSIFICATION BRANCH. TOP RESULTS ARE HIGHLIGHTED IN BOLD. QUANTITATIVE RESULTS ON THE ‘VISIBLE’ AND ‘THERMAL’ TESTING SEQUENCES OF THE DATASET VT-TINY-MOT ARE DISPLAYED, WITH THE TOP RESULTS HIGHLIGHTED IN BOLD.

	Method	HOTA↑	MOTA↑	MOTP↑	MT↑	ML ↓	FP ↓	FN ↓	IDF1↑	IDs↓
Visible	Single	26.4	29.6	56.5	184	400	16133	105952	36.1	4460
	Ours	29.1	32.0	55.6	226	444	11594	109500	43.2	1233
Thermal	Single	20.8	18.7	49.6	95	558	15783	135569	30.4	1945
	Ours	23.1	21.3	51.5	155	588	12516	135197	35.3	844

3.8/4.4% higher IDF1 for the visible and thermal modalities, respectively. Although our tracker does not achieve the best results on some specific metrics such as false positives (FP) and identity switches (IDs), it is important to consider the trade-off between false positives and false negatives (FN). Some methods such as FairMOT and Transcenter may achieve lower FP at the expense of high FN, resulting in the loss of many targets. This trade-off is a critical aspect for trackers.

The tracking performance of three RGB-T trackers is also reported in Table V. HGT-Track demonstrates an improvement of 2.8% and 2.4% at HOTA compared to ProbEn-M+SORT

in the two modalities, respectively. Trackers using RGB-T detectors can achieve lower false positives (FP) and false negatives (FN) compared to trackers using single-modality detector (Faster R-CNN). However, the tracking performance is limited due to the underutilization of temporal information, which is specifically addressed in our method.

To demonstrate the effectiveness of HGT module in integrating spatial and temporal information, we trained our method with single modality information, denoted as HGT-Track-V and HGT-Track-T. Compared with the graph-based tracker GSDT, HGT-Track-V achieves higher tracking performance (MOTA: 18.3% ↑) and higher tracking speed (FPS: 13.9 ↑). GSDT crops target patches from past frames to enhance current features. However, the crop operation costs additional time and may introduce more background noise considering the limited size of target. For the offline graph-based method MPNTrack, our method also achieved an improvement of 23.7/23.6% improvement at MOTA in visible and thermal modalities, respectively. The main reason is that the MPNTrack associate target depending on discriminative target ID feature, which is hard to learn in remote sensed scenarios.

Our proposed method is specifically designed for multi-modal data and leverages the complementary information between modalities to improve tracking performance. The

results demonstrate that our approach achieves strong tracking performance for various types of objects in different environmental conditions. Note that, to the best of our knowledge, existing public Multiple Object Tracking (MOT) datasets in the field of remote sensing are predominantly single-modal. Therefore, comparisons with other state-of-the-art methods on single-modal public datasets are not included to ensure fairness.

VII. CONCLUSION

In this paper, we introduce a unified large-scale visible-thermal benchmark named VT-Tiny-MOT for multiple tiny object tracking. We also present a novel Joint Detection and Tracking (JDT) tracker called HGT-Track, which effectively integrates complementary information from both visible and thermal modalities to track objects. HGT-Track utilizes Heterogeneous Graph Transformer encoder and decoder to integrate information across modalities. The information flows through our spatial confined heterogeneous graph, where the edge is built dependant on modality and spatial distance. This sparse information integration approach improves the efficiency of our tracking method and excludes pixel matching error between two modalities. Additionally, we introduce the ReDet module to ensure the consistency of target trajectories between different modalities, effectively reducing false negatives. Our proposed method achieves the best performance compared to other state-of-the-art trackers on the VT-Tiny-MOT dataset.

REFERENCES

- [1] C. Luo, X. Yang, and A. Yuille, "Exploring simple 3d multi-object tracking for autonomous driving," in *ICCV*, 2021.
- [2] A. K. Dasika and P. Paruchuri, "Cb+ nn ensemble to improve tracking accuracy in air surveillance," in *AAAI*, 2022.
- [3] X. Weng, Y. Yuan, and K. Kitani, "Ptp: Parallelized tracking and prediction with graph neural networks and diversity sampling," *RAL*, 2021.
- [4] C. Michaelis, B. Mitzkus, R. Geirhos, E. Rusak, O. Bringmann, A. S. Ecker, M. Bethge, and W. Brendel, "Benchmarking robustness in object detection: Autonomous driving when winter is coming," *arXiv preprint arXiv:1907.07484*, 2019.
- [5] C. Li, H. Cheng, S. Hu, X. Liu, J. Tang, and L. Lin, "Learning collaborative sparse representation for grayscale-thermal tracking," *TIP*, 2016.
- [6] C. Wang, C. Xu, Z. Cui, L. Zhou, T. Zhang, X. Zhang, and J. Yang, "Cross-modal pattern-propagation for rgb-t tracking," in *CVPR*, 2020.
- [7] Y. Zhu, C. Li, J. Tang, and B. Luo, "Quality-aware feature aggregation network for robust rgbt tracking," *TIV*, 2020.
- [8] P. Zhang, J. Zhao, D. Wang, H. Lu, and X. Ruan, "Visible-thermal uav tracking: A large-scale benchmark and new baseline," in *CVPR*, 2022.
- [9] N. Wojke, A. Bewley, and D. Paulus, "Simple online and realtime tracking with a deep association metric," in *ICIP*, 2017.
- [10] P. Bergmann, T. Meinhardt, and L. Leal-Taixe, "Tracking without bells and whistles," in *ICCV*, 2019.
- [11] C. Xiao, Q. Yin, X. Ying, R. Li, S. Wu, M. Li, L. Liu, W. An, and Z. Chen, "Dsfnet: Dynamic and static fusion network for moving object detection in satellite videos," *GRSL*, 2021.
- [12] Y. Zhang, P. Sun, Y. Jiang, D. Yu, F. Weng, Z. Yuan, P. Luo, W. Liu, and X. Wang, "Bytetrack: Multi-object tracking by associating every detection box," in *ECCV*, 2022.
- [13] J. Cao, J. Pang, X. Weng, R. Khirodkar, and K. Kitani, "Observation-centric sort: Rethinking sort for robust multi-object tracking," in *CVPR*, 2023.
- [14] Y.-T. Chen, J. Shi, Z. Ye, C. Mertz, D. Ramanan, and S. Kong, "Multimodal object detection via probabilistic ensembling," in *ECCV*, 2022.
- [15] Y. Sun, B. Cao, P. Zhu, and Q. Hu, "Drone-based rgb-infrared cross-modality vehicle detection via uncertainty-aware learning," *TCSVT*, 2022.
- [16] L. Kong, Z. Yan, Y. Zhang, W. Diao, Z. Zhu, and L. Wang, "Cfracker: Multi-object tracking with cross-frame connections in satellite videos," *TGRS*, 2023.
- [17] Y. Wang, K. Kitani, and X. Weng, "Joint object detection and multi-object tracking with graph neural networks," in *ICRA*, 2021.
- [18] Z. Hu, Y. Dong, K. Wang, and Y. Sun, "Heterogeneous graph transformer," in *WWW*, 2020.
- [19] J. Li, L. Wei, F. Zhang, T. Yang, and Z. Lu, "Joint deep and depth for object-level segmentation and stereo tracking in crowds," *TMM*, 2019.
- [20] D. Roy, Y. Li, T. Jian, P. Tian, K. R. Chowdhury, and S. Ioannidis, "Multi-modality sensing and data fusion for multi-vehicle detection," *TMM*, 2022.
- [21] Z. Liu, Y. Shang, T. Li, G. Chen, Y. Wang, Q. Hu, and P. Zhu, "Robust multi-drone multi-target tracking to resolve target occlusion: A benchmark," *TMM*, 2023.
- [22] T. T. Nguyen, H. H. Nguyen, M. Sartipi, and M. Fischella, "Multi-vehicle multi-camera tracking with graph-based tracklet features," *TMM*, 2023.
- [23] A. Lukezic, U. Kart, J. Kapyla, A. Durmush, J.-K. Kamarainen, J. Matas, and M. Kristan, "Cdtb: A color and depth visual object tracking dataset and benchmark," in *ICCV*, 2019.
- [24] X. Chen, T. Zhang, Y. Wang, Y. Wang, and H. Zhao, "Futr3d: A unified sensor fusion framework for 3d detection," in *CVPR*, 2023.
- [25] S. Zhai, P. Shao, X. Liang, and X. Wang, "Fast rgb-t tracking via cross-modal correlation filters," *Neurocomputing*, 2019.
- [26] H. Nam and B. Han, "Learning multi-domain convolutional neural networks for visual tracking," in *CVPR*, 2016.
- [27] Y. Zhu, C. Li, B. Luo, J. Tang, and X. Wang, "Dense feature aggregation and pruning for rgbt tracking," in *ACM MM*, 2019.
- [28] C. Li, L. Liu, A. Lu, Q. Ji, and J. Tang, "Challenge-aware rgbt tracking," in *ECCV*, 2020.
- [29] X. Wang, X. Shu, S. Zhang, B. Jiang, Y. Wang, Y. Tian, and F. Wu, "Mfgnet: Dynamic modality-aware filter generation for rgb-t tracking," *TMM*, 2022.
- [30] A. Lu, C. Qian, C. Li, J. Tang, and L. Wang, "Duality-gated mutual condition network for rgbt tracking," *TNNLS*, 2022.
- [31] C. Long Li, A. Lu, A. Hua Zheng, Z. Tu, and J. Tang, "Multi-adapter rgbt tracking," in *ICCVW*, 2019.
- [32] J. Redmon, S. Divvala, R. Girshick, and A. Farhadi, "You only look once: Unified, real-time object detection," in *CVPR*, 2016.
- [33] X. Zhou, D. Wang, and P. Krähenbühl, "Objects as points," *arXiv preprint arXiv:1904.07850*, 2019.
- [34] X. Zhu, W. Su, L. Lu, B. Li, X. Wang, and J. Dai, "Deformable detr: Deformable transformers for end-to-end object detection," in *ICLR*, 2020.
- [35] G. Wang, Y. Wang, R. Gu, W. Hu, and J.-N. Hwang, "Split and connect: A universal tracklet booster for multi-object tracking," *TMM*, 2022.
- [36] P. Sun, J. Cao, Y. Jiang, R. Zhang, E. Xie, Z. Yuan, C. Wang, and P. Luo, "Transtrack: Multiple object tracking with transformer," *arXiv preprint arXiv:2012.15460*, 2020.
- [37] X. Zhou, V. Koltun, and P. Krähenbühl, "Tracking objects as points," in *ECCV*, 2020.
- [38] Y. Zhang, C. Wang, X. Wang, W. Zeng, and W. Liu, "Fairmot: On the fairness of detection and re-identification in multiple object tracking," *IJCV*, 2021.
- [39] P. Chu, J. Wang, Q. You, H. Ling, and Z. Liu, "Transmot: Spatial-temporal graph transformer for multiple object tracking," in *WACV*, 2023.
- [40] I. Papakis, A. Sarkar, and A. Karpatne, "Gcnmatch: Graph convolutional neural networks for multi-object tracking via sinkhorn normalization," *arXiv preprint arXiv:2010.00067*, 2020.
- [41] Q. He, X. Sun, Z. Yan, B. Li, and K. Fu, "Multi-object tracking in satellite videos with graph-based multitask modeling," *TGRS*, 2022.
- [42] G. Brasó and L. Leal-Taixé, "Learning a neural solver for multiple object tracking," in *CVPR*, 2020.
- [43] G. Wang, R. Gu, Z. Liu, W. Hu, M. Song, and J.-N. Hwang, "Track without appearance: Learn box and tracklet embedding with local and global motion patterns for vehicle tracking," in *ICCV*, 2021.
- [44] S. M. Marvasti-Zadeh, J. Khaghani, H. Ghanei-Yakhdan, S. Kasaei, and L. Cheng, "Comet: context-aware iou-guided network for small object tracking," in *ACCV*, 2020.
- [45] N. Jiang, K. Wang, X. Peng, X. Yu, Q. Wang, J. Xing, G. Li, Q. Ye, J. Jiao, Z. Han *et al.*, "Anti-uav: A large-scale benchmark for vision-based uav tracking," *TMM*, 2021.

[46] Y. Zhu, C. Li, Y. Liu, X. Wang, J. Tang, B. Luo, and Z. Huang, "Tiny object tracking: A large-scale dataset and a baseline," *TNNLS*, 2023.

[47] B.-T. Vo and B.-N. Vo, "Labeled random finite sets and multi-object conjugate priors," *TSP*, 2013.

[48] Á. F. García-Fernández, J. L. Williams, K. Granström, and L. Svensson, "Poisson multi-bernoulli mixture filter: Direct derivation and implementation," *TAES*, 2018.

[49] W. Wang, E. Xie, X. Li, D.-P. Fan, K. Song, D. Liang, T. Lu, P. Luo, and L. Shao, "Pyramid vision transformer: A versatile backbone for dense prediction without convolutions," in *ICCV*, 2021.

[50] B. Li, C. Xiao, L. Wang, Y. Wang, Z. Lin, M. Li, W. An, and Y. Guo, "Dense nested attention network for infrared small target detection," *TIP*, 2022.

[51] A. Vaswani, N. Shazeer, N. Parmar, J. Uszkoreit, L. Jones, A. N. Gomez, Ł. Kaiser, and I. Polosukhin, "Attention is all you need," *NeurIPS*, 2017.

[52] F. Yu, D. Wang, E. Shelhamer, and T. Darrell, "Deep layer aggregation," in *CVPR*, 2018.

[53] H. W. Kuhn, "The hungarian method for the assignment problem," *NRL*, 1955.

[54] T.-Y. Lin, P. Goyal, R. Girshick, K. He, and P. Dollár, "Focal loss for dense object detection," in *ICCV*, 2017.

[55] H. Law and J. Deng, "Cornernet: Detecting objects as paired keypoints," in *ECCV*, 2018.

[56] Z. Zhang, "A flexible new technique for camera calibration," *TPAMI*, 2000.

[57] L. Wang, Y. Guo, Y. Wang, Z. Liang, Z. Lin, J. Yang, and W. An, "Parallax attention for unsupervised stereo correspondence learning," *TPAMI*, 2020.

[58] P. Dendorfer, H. Rezatofighi, A. Milan, J. Shi, D. Cremers, I. Reid, S. Roth, K. Schindler, and L. Leal-Taixé, "Mot20: A benchmark for multi object tracking in crowded scenes," *arXiv preprint arXiv:2003.09003*, 2020.

[59] T.-Y. Lin, M. Maire, S. Belongie, J. Hays, P. Perona, D. Ramanan, P. Dollár, and C. L. Zitnick, "Microsoft coco: Common objects in context," in *ECCV*, 2014.

[60] M. Kristan, J. Matas, A. Leonardis, M. Felsberg, R. Pflugfelder, J.-K. Kamarainen, L. Čehovin Zajc, O. Drbohlav, A. Lukežič, A. Berg *et al.*, "The seventh visual object tracking vot2019 challenge results," in *ICCVW*, 2019.

[61] C. Li, X. Liang, Y. Lu, N. Zhao, and J. Tang, "Rgb-t object tracking: Benchmark and baseline," *PR*, 2019.

[62] C. Li, W. Xue, Y. Jia, Z. Qu, B. Luo, J. Tang, and D. Sun, "Lasher: A large-scale high-diversity benchmark for rgbt tracking," *TIP*, 2021.

[63] Y. Xu, Y. Ban, G. Delorme, C. Gan, D. Rus, and X. Alameda-Pineda, "Transcenter: Transformers with dense representations for multiple-object tracking," *TPAMI*, 2022.

[64] J. Wu, J. Cao, L. Song, Y. Wang, M. Yang, and J. Yuan, "Track to detect and segment: An online multi-object tracker," in *CVPR*, 2021.

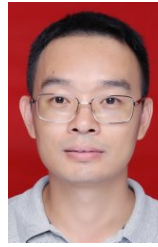
[65] R. Girshick, "Fast r-cnn," in *ICCV*, 2015.



Qingyu Xu received the B.E. degree in Electrical Engineering from Shandong University (SDU), Jinan, China, in 2015, and the M.E. degree in Information and Communication Engineering from National University of Defense Technology (NUDT), Changsha, China, in 2021. He is currently pursuing the Ph.D. degree with the College of Electronic Science and Technology, NUDT. His current research interests include information fusion and object tracking.



Longguang Wang received the B.E. degree in Electrical Engineering from Shandong University (SDU), Jinan, China, in 2015, and the Ph.D. degree in Information and Communication Engineering from National University of Defense Technology (NUDT), Changsha, China, in 2022. His current research interests include low-level vision and 3D vision.



Weidong Sheng received the Ph.D. degree from the National University of Defense Technology (NUDT), Changsha, China, in 2011. He is currently an Associate Professor with the College of Electronic Science and Technology, NUDT. His current research interests include image processing and data fusion.



Yingqian Wang received the B.E. degree in electrical engineering from Shandong University, Jinan, China, in 2016, and the master's and Ph.D. degrees in information and communication engineering from the National University of Defense Technology (NUDT), Changsha, China, in 2018 and 2023, respectively.

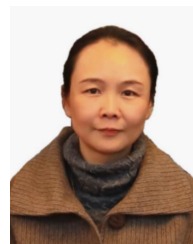
He is currently an Assistant Professor with the College of Electronic Science and Technology, NUDT. His research interests focus on optical imaging and detection, particularly on light field imaging, image super-resolution, and infrared small target detection.



Chao Xiao received the BE degree in the communication engineering and the Ph.D. degree in information and communication engineering from the National University of Defense Technology (NUDT), Changsha, China in 2016 and 2023, respectively. His research interests include deep learning, small object detection and multiple object tracking.



Chao Ma received the Ph.D. degree in information and communication engineering from the National University of Defense Technology (NUDT), Changsha, China, in 2019. He is currently an Associate Researcher with the College of Electronic Science and Technology, NUDT. His research interests include remote sensing processing, target tracking, information fusion and 3D vision.



Wei An received the Ph.D. degree from the National University of Defense Technology (NUDT), Changsha, China, in 1999. She was a Senior Visiting Scholar with the University of Southampton, Southampton, U.K., in 2016. She is currently a Professor with the College of Electronic Science and Technology, NUDT. She has authored or co-authored over 100 journal and conference publications. Her current research interests include signal processing and image processing.